Gauss–Seidel Iterative Solution of Electromagnetic Pulse Coupling to Three-Conductor Transmission Lines

Gauss–Seidel Iterative Solution of Electromagnetic Pulse Coupling to Three-Conductor Transmission Lines

Jun Guo, Yan-zhao Xie, and Flavio G. Canavero

***Abstract*—This paper proposes a distributed analytical representation and Gauss–Seidel iterative technique (Seidel-DARIT-field), which has a faster convergence rate than the Jacobi-DARIT-field method in the simulation of electromagnetic pulse (EMP) radiated field coupling to multiconductor transmission lines (MTLs) and is more valid and accurate. The process of the first iteration in this method is similar to that in the Jacobi-DARIT-field method. At the second iteration and after, every line will be updated based on the present iteration state of other lines.**

***Index Terms*—Analytical solution, electromagnetic pulse, Gauss–Seidel iteration, iterative method, transient analysis, transmission-line modeling, waveform relaxation.**

I. Introduction

THE electromagnetic pulse (EMP) field could couple to multiconductor transmission lines (MTLs), and would lead to high amplitude of the voltage and current response and put the connected electronic equipment at risk. Therefore, it is of high significance to investigate in this kind of field-wire coupling phenomenon and to predict the voltage and current response of MTLs.

Much of the research has been done on this issue [1]–[6]. In 2013, Y.-z. Xie, J. Guo, and F. Canavero proposed the Jacobi-DARIT-field method [7] for the field-wire coupling analysis. Based on the Waveform Relaxation and Transverse Partitioning (WR-TP, [8]–[24]) algorithm, this method adopts an analytical Jacobi iterative way. Therefore, the high computational efficiency and good simulation accuracy could be obtained after only a few iteration steps in most situations such as in the case of interconnected lines on PCB.

However, when using this method in the cases, which have big number of conductors or the power distribution lines as shown in Fig. 1, only a few iteration steps were insufficient due to the decrease of the convergence rate. As the Jacobi-DARIT-field method did not use all the updated informations in the iteration process, to speed up the convergence rate of the DARIT-field method, this paper developed the Seidel-DARIT-field method, which could make the maximum use of the updated informations in every iteration step. Similar to the Jacobi-DARIT-field method, the first iteration in the Seidel-DARIT-field method is to deal with the incoming EMP wave interacting with each line independently. At the second iteration and after, the voltage and current informations of adjacent lines used are obtained from the results of front lines, which is updated in this iteration step, and of after lines, which is updated in previous iteration step. When adopting this method in the power distribution line case, the result shows a better performance compared with the Jacobi method.

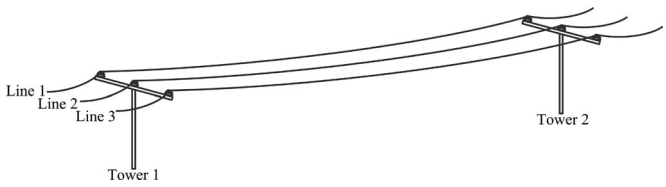

Fig. 1. Structure of the power distribution line.

The rest of this paper is organized as follows. Section II introduces the basic idea of proposed Seidel-DARIT-field approach briefly. Section III explains the derived formulae in detail. Sections IV and V present the validation examples and conclusions, respectively.

II. Scheme of the Seidel-DARIT-Field Method

The problem to be investigated is that the incoming EMP plane wave radiated to the MTLs, which terminates with linear loads. Similar to the Jacobi-DARIT-field method, the process of the Seidel-DARIT-field method begins from the frequency-domain Telegrapher's equations in the matrix form. By resolving the equations and applying waveform relaxation techniques to it, a recursive set of decoupled differential equations based on the Gauss–Seidel iteration for line i are obtained

$$\begin{aligned}\frac{dv_i^{(r+1)}(x,s)}{dx}+z'_{ii}(s)i_i^{(r+1)}(x,s)&=e_{A,i}^{(r+1)}(x,s)+e_{B,i}(x,s)\\ \frac{di_i^{(r+1)}(x,s)}{dx}+y'_{ii}(s)v_i^{(r+1)}(x,s)&=q_{A,i}^{(r+1)}(x,s)+q_{B,i}(x,s).\end{aligned}\tag{1}$$

where $(r+1)$ represents the $(r+1)$th iteration, $r\geq 0$. Note that, there are two parts on the right-hand side of the equations.

The first part $'A'$ ($e_{A,i}^{(r)}$ and $q_{A,i}^{(r)}$) of ith line is the iterative term, which represents the neighboring effects due to the influence of

Jun Guo and Yan-zhao Xie are with the State Key Laboratory of Electrical Insulation and Power Equipment, School of Electrical Engineering, Xi'an Jiaotong University, Xi'an 710049, China (e-mail: gjgjgj@stu.xjtu.edu.cn; yanzhao.XIE@gmail.com).

Flavio Canavero is with the EMC Group, Department of Electronics, Politecnico Di Torino, Turin 10129, Italy (e-mail: flavio.canavero@polito.it).

the adjacent lines and is updated in each iteration step, and it is the main difference compared with the Jacobi-DARIT-field method. Based on the Gauss – Seidel iteration algorithm, this part would be updated on the basis of the state of line $1\sim i-1$ at the present iteration and line $i+1\sim N$ at the previous iteration. Depending upon the value of i, the expressions of $e_{A,i}^{(r)}$ and $q_{A,i}^{(r)}$ are as follows.

1) *Case 1:* For $(i=1)$

$$\begin{aligned} e_{A,i}^{(r+1)}(x,s) =& -\sum_{j=2}^{N} z'_{ij}(s) i_j^{(r)}(x,s) \\ q_{A,i}^{(r+1)}(x,s) =& -\sum_{j=2}^{N} y'_{ij}(s) v_j^{(r)}(x,s). \end{aligned} \tag{2}$$

2) *Case 2:* For $(1<i<N)$

$$\begin{aligned} e_{A,1}^{(r+1)}(x,s) =& -\sum_{j=1}^{i-1} z'_{1j}(s) i_j^{(r+1)}(x,s) \\ & -\sum_{j=i+1}^{N} z'_{1j}(s) i_j^{(r)}(x,s) \\ q_{A,1}^{(r+1)}(x,s) =& -\sum_{j=1}^{i-1} y'_{ij}(s) v_j^{(r+1)}(x,s) \\ & -\sum_{j=i+1}^{N} y'_{ij}(s) v_j^{(r)}(x,s). \end{aligned} \tag{3}$$

3) *Case 3:* For $(i=N)$

$$\begin{aligned} e_{A,1}^{(r+1)}(x,s) =& -\sum_{j=1}^{N-1} z'_{1j}(s) i_j^{(r+1)}(x,s) \\ q_{A,1}^{(r+1)}(x,s) =& -\sum_{j=1}^{N-1} y'_{ij}(s) v_j^{(r+1)}(x,s). \end{aligned} \tag{4}$$

The second part $'B'$ ($e_{B,i}^{(r)}$ and $q_{B,i}^{(r)}$) is the general term due to the excitation of incoming EMP wave, which has the same form as that in the Jacobi-DARIT-field method.

The load responses would be calculated with the BLT equation [25]. The main task of each iteration step is to get the source terms $S_{i+}^{(r)}$ and $S_{i-}^{(r)}$, which are in BLT equation as input parameters

$$\begin{aligned} \begin{bmatrix} S_{i+}^{(r)} \\ S_{i-}^{(r)} \end{bmatrix} &= \begin{bmatrix} \int_0^L e^{-\gamma_i (L-x')} [e_i^{(r)}(x',s) + z_{c,i} q_i^{(r)}(x',s)] dx' \\ -\int_0^L e^{-\gamma_i x'} [e_i^{(r)}(x',s) - z_{c,i} q_i^{(r)}(x',s)] dx' \end{bmatrix} \\ &= \begin{bmatrix} S_{i+,A} + S_{i+,B} \\ S_{i-,A} + S_{i-,B} \end{bmatrix}. \end{aligned} \tag{5}$$

III. Mathematical Derivation of the Proposed Seidel-DARIT-Field Algorithm

All the expressions in Seidel-DARIT-field method should be derived as new ones because of the iterative scheme it adopts is different from Jacobi-DARIT-field method. In this section, the MTLs model with three conductors would be considered and the formulae of three iterations would be derived.

A. Iteration 1

At this iteration, there are no coupling effects from the neighboring lines since the initial states of the lines are zeros, which is the same as in the Jacobi-DAARIT-field method (the expressions in iteration 1 can be seen in [7]).

B. Iteration 2

From this step on, each line is excited by the incoming EMP wave and the coupling effects of all the other adjacent lines. For the voltages and currents on the mth line, we have

$$\begin{aligned} \frac{dv_m^{(2)}(x)}{dx} + z'_{mm} i_m^{(2)}(x) =& \; e_{m,A}^{(2)}(x) + V'_m(x) \\ \frac{di_m^{(2)}(x)}{dx} + y'_{mm} v_m^{(2)}(x) =& \; q_{m,A}^{(2)}(x) + I'_m(x). \end{aligned} \tag{6}$$

Since the Gauss–Seidel iteration method is adopted, the expression form of $e_{m,A}^{(2)}(x)$ and $q_{m,A}^{(2)}(x)$ are different in each conductor, and we compute them one after another.

1) Conductor #1: When analyzing the state of line 1, the voltage and current states of the other adjacent lines used are obtained from iteration 1 for line 2 and 3. The virtual p.u.l. distributed voltage and current sources due to the effects of adjacent lines are

$$e_{1,A}^{(2)}(x) = -\sum_{m=2}^{3} z'_{1m} i_m^{(1)}(x) \quad q_{1,A}^{(2)}(x) = -\sum_{m=2}^{3} y'_{1m} v_m^{(1)}(x). \tag{7}$$

After we get the expressions of the combined voltage source wave $\left(S_{1+,A}^{(2)}(x)\right)$ and $\left(S_{1-,A}^{(2)}(x)\right)$, the corresponding elements in the source vector of part A may be given as follows:

$$\begin{aligned} S_{1+,A}^{(2)} =& \; e^{-\gamma_1 L}\Big[-\sum_{m=2}^{3} \Big(B_{1+}^{(2)}(1,m) Q_{1+,m}^{(2)} \\ & + B_{2+}^{(2)}(n,m) K_{1+,m+} + B_{3+}^{(2)}(n,m) K_{1+} \Big) \Big] \\ S_{1-,A}^{(2)} =& \sum_{m=2}^{3} \Big(B_{1-}^{(2)}(1,m) K_{1-,m-} \\ & + B_{2-}^{(2)}(1,m) Q_{1-,m}^{(2)} + B_{3-}^{(2)}(1,m) K_{1-} \Big). \end{aligned} \tag{8}$$

where, in order to abbreviate the length of the formulae, we use the notations as follows:

$$\begin{aligned} K_{n+,m+} =& \; \frac{e^{(\gamma_n+\gamma_m)L} - 1}{\gamma_n + \gamma_m} \\ K_{n+,m-} =& \; \frac{e^{(\gamma_n-\gamma_m)L} - 1}{\gamma_n - \gamma_m} \\ K_{n-,m+} =& \; \frac{e^{(\gamma_m-\gamma_n)L} - 1}{\gamma_m - \gamma_n} \end{aligned}$$

$$
\begin{aligned}
K_{n-,m-} &= \frac{e^{(-\gamma_n-\gamma_m)L}-1}{-\gamma_n-\gamma_m} \\
K_{n+} &= \frac{e^{-(\gamma_n+jk\cos\psi\cos\phi)L}-1}{-(\gamma_n+jk\cos\psi\cos\phi)}; \\
K_{n-} &= \frac{e^{(\gamma_n-jk\cos\psi\cos\phi)L}-1}{\gamma_n-jk\cos\psi\cos\phi} \\
B_{l+}^{(r+1)}(n,m) &= \left(z'_{nm}f_{i_l}^{(r)}(m)+z_{c,n}y'_{nm}f_{v_l}^{(r)}(m)\right) \\
B_{l-}^{(r+1)}(n,m) &= \left(z'_{nm}f_{i_l}^{(r)}(m)-z_{c,n}y'_{nm}f_{v_l}^{(r)}(m)\right).
\end{aligned} \tag{9}
$$

In order to implement the iterating procedure, the symmetry of the MTLs, which indicates whether the propagation constants of one line is equal to the other's, should be considered. The values of $Q_{1+,m}^{(2)}$ and $Q_{1-,m}^{(2)}$ are determined depending upon the symmetry as follows.

1) *Unsymmetrical Cases of MTLs ($\gamma_n \neq \gamma_m$)*

$$
Q_{1+,m}^{(2)} = K_{n+,m-}, \qquad Q_{1-,m}^{(2)} = K_{n-,m+}. \tag{10}
$$

2) *Symmetrical Cases of MTLs ($\gamma_k = \gamma_g$, the case of $k = g$ included)*

$$
Q_{1+,m}^{(2)} = L, \qquad Q_{1-,m}^{(2)} = L. \tag{11}
$$

The load responses could be solved by means of the BLT equation. Then, incorporating the terminal conditions, the voltage $v_1(x)$ and current $i_1(x)$ can be obtained. They are given as follows:

$$
\begin{aligned}
v_1^{(2)}(x) = {} & f_{v_1}^{(2)}(1)e^{-\gamma_1 x}+f_{v_2}^{(2)}(1)e^{\gamma_1 x}+f_{v_3}^{(2)}(1)e^{-jk\cos\psi\phi x} \\
& +f_{v_4}^{(2)}(1)xe^{-\gamma_1 x}+f_{v_5}^{(2)}(1)xe^{\gamma_1 x}+f_{v_6}^{(2)}(1)e^{-\gamma_2 x} \\
& +f_{v_7}^{(2)}(1)e^{\gamma_2 x}+f_{v_8}^{(2)}(1)e^{-\gamma_3 x}+f_{v_9}^{(2)}(1)e^{\gamma_3 x} \\
i_1^{(2)}(x) = {} & f_{i_1}^{(2)}(1)e^{-\gamma_1 x}+f_{i_2}^{(2)}(1)e^{\gamma_1 x}+f_{i_3}^{(2)}(1)e^{-jk\cos\psi\phi x} \\
& +f_{i_4}^{(2)}(1)xe^{-\gamma_1 x}+f_{i_5}^{(2)}(1)xe^{\gamma_1 x}+f_{i_6}^{(2)}(1)e^{-\gamma_2 x} \\
& +f_{i_7}^{(2)}(1)e^{\gamma_2 x}+f_{i_8}^{(2)}(1)e^{-\gamma_3 x}+f_{i_9}^{(2)}(1)e^{\gamma_3 x}
\end{aligned} \tag{12}
$$

where $f_{v_{1\sim9}}^{(2)}, f_{i_{1\sim9}}^{(2)}$ are the predefined coefficients depending upon whether the case is symmetrical or not.

2) Conductor #2: When calculating the state of line 2, the voltage and current states of the other adjacent lines used are obtained from iteration 2 for line 1 and iteration 1 for line 3. The virtual p.u.l. distributed voltage and current sources due to the adjacent lines are

$$
\begin{aligned}
e_{2,A}^{(2)}(x) &= -z'_{21}i_1^{(2)}(x)-z'_{23}i_3^{(1)}(x), \\
q_{2,A}^{(2)}(x) &= -y'_{21}v_1^{(2)}(x)-y'_{23}v_3^{(1)}(x).
\end{aligned} \tag{13}
$$

The derivation in detail is given in Appendix A.

In this step, the voltage and current on line 2 are expressed by $v_2(x)$ and $i_2(x)$, respectively. They are given as follows:

$$
\begin{aligned}
v_2^{(2)}(x) = {} & f_{v_1}^{(2)}(2)e^{-\gamma_2 x}+f_{v_2}^{(2)}(2)e^{\gamma_2 x}+f_{v_3}^{(3)}(2)e^{-jk\cos\psi\cos\phi x} \\
& +f_{v_4}^{(2)}(2)e^{-\gamma_1 x}+f_{v_5}^{(2)}(2)e^{\gamma_1 x}+f_{v_6}^{(2)}(2)xe^{-\gamma_2 x} \\
& +f_{v_7}^{(2)}(2)xe^{\gamma_2 x}+f_{v_8}^{(2)}(2)xe^{-\gamma_1 x}+f_{v_9}^{(2)}(2)xe^{\gamma_1 x} \\
& +f_{v_{10}}^{(2)}(2)e^{-\gamma_3 x}+f_{v_{11}}^{(2)}(2)e^{\gamma_3 x} \\
i_2^{(2)}(x) = {} & f_{i_1}^{(2)}(2)e^{-\gamma_2 x}+f_{i_2}^{(2)}(2)e^{\gamma_2 x}+f_{i_3}^{(3)}(2)e^{-jk\cos\psi\cos\phi x} \\
& +f_{i_4}^{(2)}(2)e^{-\gamma_1 x}+f_{i_5}^{(2)}(2)e^{\gamma_1 x}+f_{i_6}^{(2)}(2)xe^{-\gamma_2 x} \\
& +f_{i_7}^{(2)}(2)xe^{\gamma_2 x}+f_{i_8}^{(2)}(2)xe^{-\gamma_1 x}+f_{i_9}^{(2)}(2)xe^{\gamma_1 x} \\
& +f_{i_{10}}^{(2)}(2)e^{-\gamma_3 x}+f_{i_{11}}^{(2)}(2)e^{\gamma_3 x}.
\end{aligned} \tag{14}
$$

where, $f_{v_{1\sim11}}^{(2)}$, $f_{i_{1\sim11}}^{(2)}$ are the predefined coefficients.

3) Conductor #3: When analyzing the state of line 3, the voltage and current states of the other adjacent lines used are obtained from iteration 2 for line 1 and 2. The virtual p.u.l. distributed voltage and current sources due to the adjacent lines are

$$
\begin{aligned}
e_{3,A}^{(2)}(x) &= -z'_{31}i_1^{(2)}(x)-z'_{32}i_2^{(2)}(x) \\
q_{3,A}^{(2)}(x) &= -y'_{31}v_1^{(2)}(x)-y'_{32}v_2^{(2)}(x).
\end{aligned} \tag{15}
$$

The derivation in detail is given in Appendix A depending upon whether the case is symmetrical or not.

In this step, the voltage and current on line 3 are expressed by $v_3(x)$ and $i_3(x)$, respectively. They are given as follows:

$$
\begin{aligned}
v_3^{(2)}(x) = {} & f_{v_1}^{(2)}(3)e^{-\gamma_3 x}+f_{v_2}^{(2)}(3)e^{\gamma_3 x}+f_{v_3}^{(2)}(3)e^{-jk\cos\psi\cos\phi x} \\
& +f_{v_4}^{(2)}(3)e^{-\gamma_2 x}+f_{v_5}^{(2)}(3)e^{\gamma_2 x}+f_{v_6}^{(2)}(3)xe^{-\gamma_1 x} \\
& +f_{v_7}^{(2)}(3)xe^{\gamma_1 x}+f_{v_8}^{(2)}(3)xe^{-\gamma_3 x}+f_{v_9}^{(2)}(3)xe^{\gamma_3 x} \\
& +f_{v_{10}}^{(2)}(3)xe^{-\gamma_2 x}+f_{v_{11}}^{(2)}(3)xe^{\gamma_2 x}+f_{v_{12}}^{(2)}(3)xe^{-\gamma_1 x} \\
& +f_{v_{13}}^{(2)}(3)xe^{\gamma_1 x}+f_{v_{14}}^{(2)}(3)x^2e^{-\gamma_2 x}+f_{v_{15}}^{(2)}(3)x^2e^{\gamma_2 x} \\
i_3^{(2)}(x) = {} & f_{i_1}^{(2)}(3)e^{-\gamma_3 x}+f_{i_2}^{(2)}(3)e^{\gamma_3 x}+f_{i_3}^{(2)}(3)e^{-jk\cos\psi\cos\phi x} \\
& +f_{i_4}^{(2)}(3)e^{-\gamma_2 x}+f_{i_5}^{(2)}(3)e^{\gamma_2 x}+f_{i_6}^{(2)}(3)xe^{-\gamma_1 x} \\
& +f_{i_7}^{(2)}(3)xe^{\gamma_1 x}+f_{i_8}^{(2)}(3)xe^{-\gamma_3 x}+f_{i_9}^{(2)}(3)xe^{\gamma_3 x} \\
& +f_{i_{10}}^{(2)}(3)xe^{-\gamma_2 x}+f_{i_{11}}^{(2)}(3)xe^{\gamma_2 x}+f_{i_{12}}^{(2)}(3)xe^{-\gamma_1 x} \\
& +f_{i_{13}}^{(2)}(3)xe^{\gamma_1 x}+f_{i_{14}}^{(2)}(3)x^2e^{-\gamma_2 x}+f_{i_{15}}^{(2)}(3)x^2e^{\gamma_2 x}.
\end{aligned} \tag{16}
$$

where $f_{v_{1\sim15}}^{(2)}$, $f_{i_{1\sim15}}^{(2)}$ are the predefined coefficients.

C. Iteration 3

The Telegrapher's equations for this step are the same as those for Iteration 2. Note that the convergence of each line is different due to the iteration sequence, and line 3 has the best computational accuracy, whereas line 1 has the worst one. In order to balance the accuracy, the inversion computation sequence is adopted in iteration 3. Except for the inversing iteration sequence, the derivation process in this iteration is similar to that in iteration 2 and would not be listed here due to the page limit.

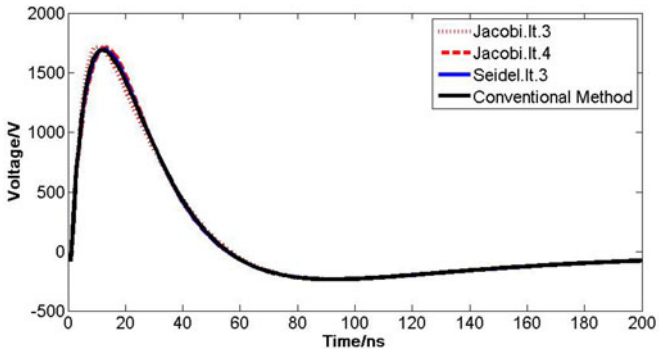

Fig. 2. Far-end response of line #1 with coupling factors of 0.05 (Example 1).

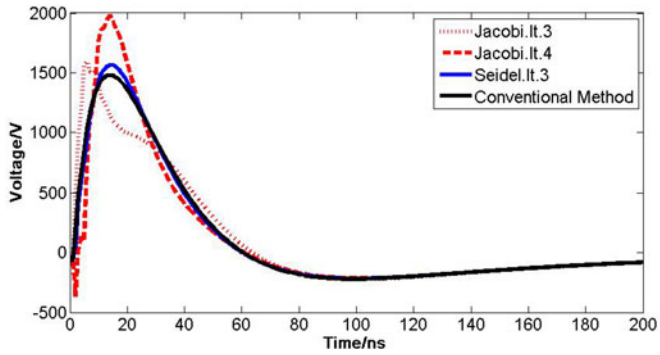

Fig. 3. Far-end response of line #1 with coupling factors of 0.5 (Example 1).

It is worthwhile to note that there should be a correction term in the expression of source term after iteration 1, which is small in ordinary case but would be larger in the high resonance case such as in the open-circuit system. To deal with this effect, some variation method and perturbation theory could be considered.

IV. Validation of the Proposed Algorithm

As described in [26], the coupling factors (CF, which was defined in [7]) and ratio of the line length over the wavelength (L/λ) are the key influence factors of the convergence in the Jacobi-DARIT-field method. The convergence speed would be low if the value of CF or L/λ is high. Therefore, two examples will be shown in this section to show the advantages of the Seidel-DARIT-field method. The first example demonstrates the performance of the Seidel-DARIT-field in handling with the high CF case. The second example illustrates the advantage of the Seidel-DARIT-field method in the power distribution line case and shows the performance of the proposed method in the cases with different line length. The MTLs structure in both the examples consists of three conductors that are above the lossy ground. The relative dielectric constant and electrical conductivity of ground are 10 and 0.01 S/m, respectively. In both the examples, MTLs are illuminated by the incoming EMP wave as defined by IEC 61000-2-9[2] and with the incidence angles of $\alpha = 0°$, $\psi = 30°$ and $\phi = 0°$.

A. Example 1: High Value of CF

This example aims to show the capability of the Seidel-DARIT-field method in handling with the high CF case and to compare its computational accuracy with the Jacobi-DARIT-field method at different CF levels. In this example, MTLs with the length of 40 cm, height of 2 cm, and diameter of 1 mm are considered. The loads on both ends are 50 Ω. There are ten cases in this example with the distance between lines ranging from 60 to 6.2 mm to make the CF range from 0.05 to 0.5 in step of 0.05. Figs. 2 and 3 show a sample of the computed waveforms from iteration 3 of the proposed Seidel-DARIT-field method and iteration 3 and 4 of the Jacobi-DARIT-field compared to the computed waveforms from the conventional stamp method. It can be seen that when CF is at a low level, the results from the two DARIT-field methods are all in good agreement with the result from the conventional stamp method. When CF is at a high level, the results show clearly that the Seidel method has a higher convergence rate than the Jacobi method.

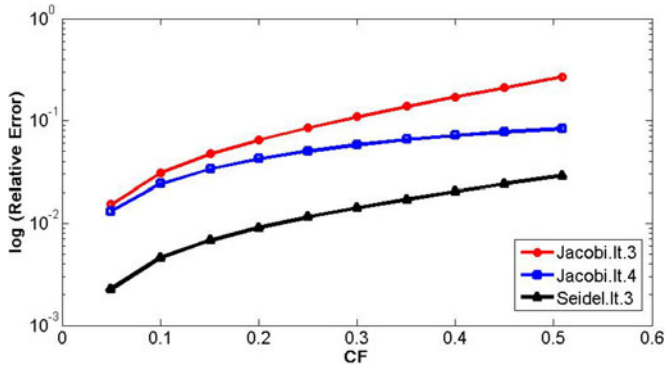

Fig. 4. Relative error of far-end response of line #1 with different coupling factors (Example 1).

In order to quantify their accuracy, the relative error ϵ based on energy norm in time domain is adopted. Fig. 4 shows the accuracy of the two DARIT-field methods with different CF. It can be seen clearly that the Seidel-DARIT-field method is more convergent than the Jacobi-DARIT-field method.

B. Example 2: High Value of L/λ

Since λ is determined in certain EMP waveform, convergence rate is highly dependent on the line length L. A 380-V power distribution line case is presented in the following. The structure of the power distribution line is shown in Fig. 1. The height of lines and distance between lines are 3 and 1.5 m, respectively. There are three lines with the type of LGJ-16/3. The loads at both ends are equal to characteristic impedance of lines. The line length is 60 m, which is the distance between two towers. Fig. 5 shows the comparison of simulation results from the Jacobi-DARIT-field method and the Seidel-DARIT-field method. From the plot, it can be seen that the results from the Jacobi method is not satisfactory, whereas the result from the Seidel method agrees well with the conventional method. When calculating relative errors, it is 34%, 21%, and 8.5% corresponding to iteration 3 and 4 of the Jacobi method and iteration 3 of the Seidel

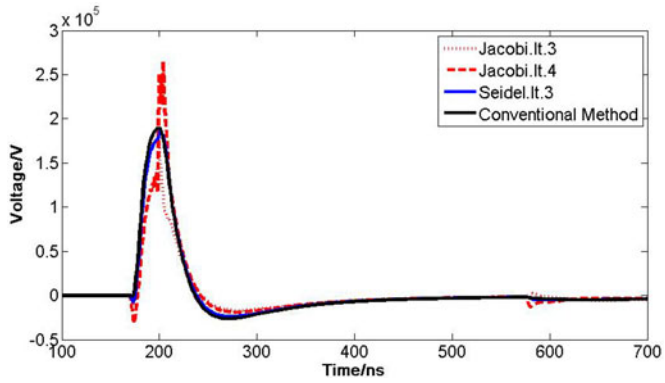

Fig. 5. Computed waveforms of far-end response of line #1 (Example 2).

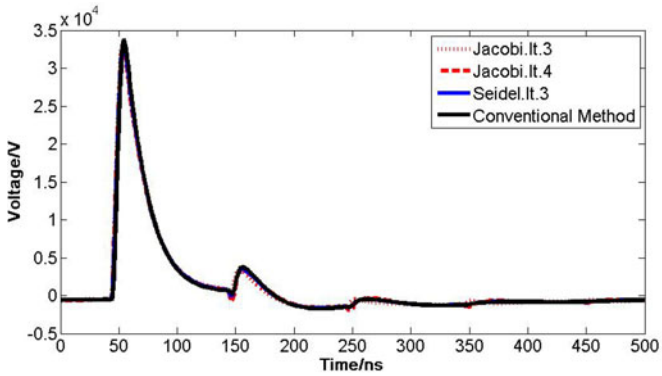

Fig. 6. Computed waveforms of far-end response of line #1 when the lines length is 15 m (Example 2: Long Wire).

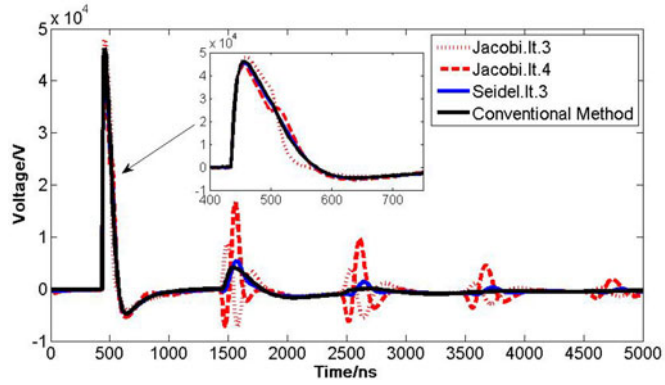

Fig. 7. Computed waveforms of far-end response of line #1 when the lines length is 150 m (Example 2: Long Wire).

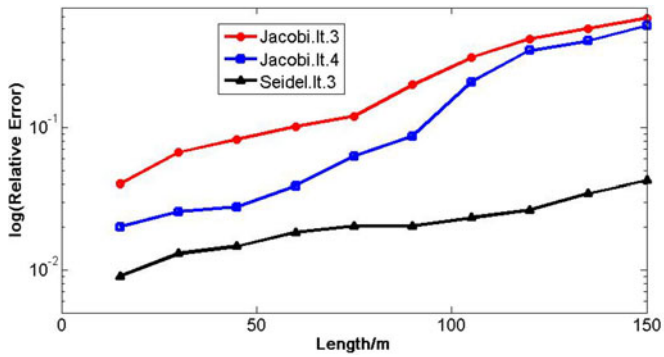

Fig. 8. Relative error of far-end response of line #1 with different length of lines (Example 2: Long Wire).

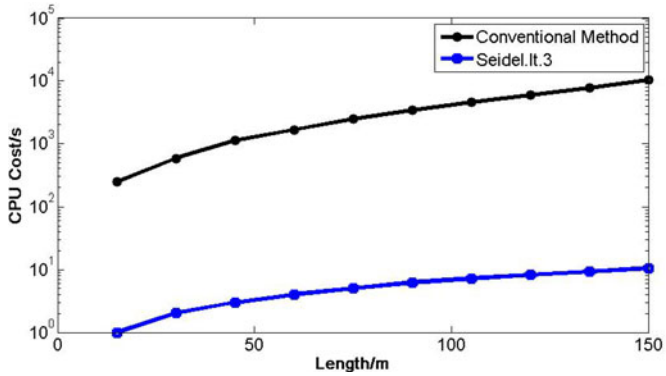

Fig. 9. Time cost of the conventional method and the Seidel method with different line length (Example 2: Long Wire).

method, respectively. It can be seen that the result from the Seidel method could meet the computational accuracy requirement well in this example.

In order to show the performances of the Seidel-DARIT-field and the Jacobi-DARIT-field method with different wire length, a set of examples with different line length were produced. In these examples, the height, distance between lines and diameter of the MTLs are 1 m, 1.5 m, and 1 mm, respectively. The loads on both ends are 100 Ω. There are ten cases with the length of lines ranging from 15 to 150 m in step of 15 m. Figs. 6 and 7 show two samples of the computed waveforms from Jacobi-iteration 3 and 4 and Seidel-iteration 3 compared to the computed waveforms from the conventional stamp method when the line length is 15 and 150 m, respectively. It can be seen that the two DARIT-field methods are all in good agreement with the conventional stamp method when the lines are relatively not so long. However, when the lines become longer, the accuracy of these two methods all declines at a different level. Despite this, the result from the Seidel method still performs a reasonable precision. Fig. 8 shows the relative errors both from Jacobi-iteration 3 and 4 and Seidel-iteration 3 with different line length L. The plot shows clearly that the accuracy of the Seidel method is better than the Jacobi method.

Since the line length is relatively long, there is a time delay in the far-end response. To ensure that the computation results are accurate and contain many reflection peaks in the waveform, the simulating time should be as long as possible. In this example, the simulating time is ten times as long as the delay time. For example, when the line length is 150 m, the delay time in the far-end response approximately equals to 500 ns, and the simulating time should be 5000 ns. However, this simulating time is so long for the conventional method because of the high CPU cost. Fig. 9 shows the CPU cost of the conventional method and the Seidel-DARIT-field method when the line length ranged from

15 to 150 m (run on PC with Core i3 CPU, 2-G RAM). The comparison would make sense since the relative error of the Seidel-DARIT-field method stays at a low level.

V. Summary and Conclusion

In this paper, the Seidel-DARIT-field method has been proposed, which provides an iterative approach to predict EMP coupling to MTLs in an analytical way. In the three-conductor models, when updating the state of line 2, the voltage and current informations of other lines used are obtained from the results of line 1 which is updated in this iteration step and of line 3 which is not updated. The validation results show that the Seidel-DARIT-field method has a high convergence rate, which makes it more accurate in some cases. However, the iterative expressions in the Seidel method may be difficult to derive in the cases which have a big number of conductors.

Future work will develop the new method in time domain to handle with the nonlinear problem.

Appendix A
Coefficients

A. Derivation of Conductor #2 in Iteration 2: The $S^{(2)}_{2+,A}$ and $S^{(2)}_{2-,A}$ are derived as follows:

$$\begin{aligned}
S^{(2)}_{2+,A} = & -e^{-\gamma_2 L}\Big[A^{(2)}_{1+}(2,1)K_{2+,1-}+A^{(2)}_{2+}(2,1)K_{2+,1+}\\
&+\big[A^{(2)}_{3+}(2,1)+B^{(2)}_{3+}(2,3)\big]K_{2+}+A^{(2)}_{4+}(2,1)KK_{2+,1-}\\
&+A^{(2)}_{5+}(2,1)KK_{2+,1+}+A^{(2)}_{6+}(2,1)L\\
&+A^{(2)}_{7+}(2,1)K_{2+,2+}+\big[A^{(2)}_{8+}(2,1)\\
&+B^{(2)}_{1+}(2,3)\big]K_{2+,3-}\\
&+\big[A^{(2)}_{9+}(2,1)+B^{(2)}_{2+}(2,3)\big]K_{2+,3+}\Big]\\
S^{(2)}_{2-,A} = & \ A^{(2)}_{1-}(2,1)K_{2-,1-}+A^{(2)}_{2-}(2,1)K_{2-,1+}\\
&+\big[A^{(2)}_{3-}(2,1)+B^{(2)}_{3-}(2,3)\big]K_{2-}+A^{(2)}_{4-}(2,1)KK_{2-,1-}\\
&+A^{(2)}_{5-}(2,1)KK_{2-,1+}+A^{(2)}_{6-}(2,1)K_{2-,2-}\\
&+A^{(2)}_{7-}(2,1)L+\big[A^{(2)}_{8-}(2,1)+B^{(2)}_{1-}(2,3)\big]K_{2-,3-}\\
&+\big[A^{(2)}_{9-}(2,1)+B^{(2)}_{2-}(2,3)\big]K_{2-,3+}. \qquad (17)
\end{aligned}$$

Where we use the notations as follows:

$$\begin{aligned}
KK_{n+,m+} &= \frac{Le^{(\gamma_n+\gamma_m)L}}{\gamma_n+\gamma_m}-\frac{e^{(\gamma_n+\gamma_m)L}-1}{(\gamma_n+\gamma_m)^2}\\
KK_{n+,m-} &= \frac{Le^{(\gamma_n-\gamma_m)L}}{\gamma_n-\gamma_m}-\frac{e^{(\gamma_n-\gamma_m)L}-1}{(\gamma_n-\gamma_m)^2}\\
KK_{n-,m+} &= \frac{Le^{(\gamma_m-\gamma_n)L}}{\gamma_m-\gamma_n}-\frac{e^{(\gamma_m-\gamma_n)L}-1}{(\gamma_m-\gamma_n)^2}\\
KK_{n-,m-} &= \frac{Le^{(-\gamma_n-\gamma_m)L}}{-\gamma_n-\gamma_m}-\frac{e^{(-\gamma_n-\gamma_m)L}-1}{(-\gamma_n-\gamma_m)^2}
\end{aligned}$$

$$\begin{aligned}
A^{(r+1)}_{l+}(n,m) &= \big(z'_{nm}f^{(r+1)}_{i_l}(m)+z_{c,n}y'_{nm}f^{(r+1)}_{v_l}(m)\big)\\
A^{(r+1)}_{l-}(n,m) &= \big(z'_{nm}f^{(r+1)}_{i_l}(m)-z_{c,n}y'_{nm}f^{(r+1)}_{v_l}(m)\big).
\end{aligned} \qquad (18)$$

Appendix B
Derivation of Conductor #3 in Iteration 2

The $S^{(2)}_{3+,A}$ and $S^{(2)}_{3-,A}$ are derived as follows:

$$\begin{aligned}
S^{(2)}_{3+,A} = & -e^{-\gamma_3 L}\Big\{\big[A^{(2)}_{1+}(3,2)+A^{(2)}_{6+}(3,1)\big]K_{3+,2-}\\
&+\big[A^{(2)}_{2+}(3,2)+A^{(2)}_{7+}(3,1)\big]K_{3+,2+}+\big[A^{(2)}_{3+}(3,2)\\
&+A^{(2)}_{3+}(3,1)\big]K_{3+}+\big[A^{(2)}_{4+}(3,2)+A^{(2)}_{1+}(3,1)\big]Q^{(2)}_{31+}\\
&+\big[A^{(2)}_{5+}(3,2)+A^{(2)}_{2+}(3,1)\big]KK_{3+,1+}+A^{(2)}_{6+}(3,2)KK_{3+,2-}\\
&+A^{(2)}_{7+}(3,2)KK_{3+,2+}+\big[A^{(2)}_{8+}(3,2)+A^{(2)}_{4+}(3,1)\big]Q^{(2)}_{32+}\\
&+\big[A^{(2)}_{9+}(3,2)+A^{(2)}_{5+}(3,1)\big]KK_{3+,1+}+\big[A^{(2)}_{10+}(3,2)\\
&+A^{(2)}_{8+}(3,1)\big]L+\big[A^{(2)}_{11+}(3,2)+A^{(2)}_{9+}(3,1)\big]K_{3+,3+}\Big\}\\
S^{(2)}_{3-,A} = & \big[A^{(2)}_{1-}(3,2)+A^{(2)}_{6-}(3,1)\big]K_{3-,2-}\\
&+\big[A^{(2)}_{2-}(3,2)+A^{(2)}_{7-}(3,1)\big]K_{3-,2+}+\big[A^{(2)}_{3-}(3,2)\\
&+A^{(2)}_{3-}(3,1)\big]K_{3-}+\big[A^{(2)}_{4-}(3,2)+A^{(2)}_{1-}(3,1)\big]K_{3-,1-}\\
&+\big[A^{(2)}_{5-}(3,2)+A^{(2)}_{2-}(3,1)\big]Q^{(2)}_{31-}+A^{(2)}_{6-}(3,2)KK_{3-,2-}\\
&+A^{(2)}_{7-}(3,2)KK_{3-,2+}+\big[A^{(2)}_{8-}(3,2)+A^{(2)}_{4-}(3,1)\big]KK_{3-,1-}\\
&+\big[A^{(2)}_{9-}(3,2)+A^{(2)}_{5-}(3,1)\big]Q^{(2)}_{32-}+\big[A^{(2)}_{10-}(3,2)\\
&+A^{(2)}_{8-}(3,1)\big]K_{3-,3-}+\big[A^{(2)}_{11-}(3,2)+A^{(2)}_{9-}(3,1)\big]L. \qquad (19)
\end{aligned}$$

The values of $Q^{(2)}_{31+}$, $Q^{(2)}_{32+}$, $Q^{(2)}_{31-}$, and $Q^{(2)}_{32-}$ are determined depending upon the symmetry as follows.[Comp: Please change a) and b) to 1) and 2), respectively, in the following. Also remove ":" before equations]

a) *Unsymmetrical Cases of MTLs ($\gamma_1 \neq \gamma_3$)*

$$\begin{aligned}
Q^{(2)}_{31+} &= K_{3+,1-}, Q^{(2)}_{32+} = KK_{3+,1-}\\
Q^{(2)}_{31-} &= K_{3-,1+}, Q^{(2)}_{32-} = KK_{3-,1+}. \qquad (20)
\end{aligned}$$

b) *Symmetrical Cases of MTLs ($\gamma_1 = \gamma_3$)*

$$Q^{(2)}_{31+} = L, Q^{(2)}_{32+} = L^2/2; Q^{(2)}_{31-} = L, Q^{(2)}_{32-} = L^2/2. \qquad (21)$$

References

[1] C. R. Paul, *Analysis of Multiconductor Transmission Lines*, 2nd ed. New York, NY, USA: Wiley, 2008.

[2] F. M. Tesche, M. V. Ianoz, and T. Karlsson, *EMC Analysis Methods and Computational Models*. New York NY, USA: Wiley, 1997.

[3] C. R. Paul, "Solution of the transmission-line equations under the weak-coupling assumption," *IEEE Trans. Electromagn. Compat.*, vol. 44, no. 3, pp. 413–423, Aug. 2002.

[4] C. E. Baum, "Low- and high-frequency solutions of the telegrapher equations for nonuniform multiconductor transmission lines," *IEEE Int. Symp. Electromagn. Compat.*, Jul. 2007, pp. 1–14.

[5] F. Canavero and I. Maio, "Transient simulation of lossy multiconductor interconnects," in *Proc. Int. Symp. Electromagn. Compat.*, May. 21–23, 1997, pp. 243–246.

[6] C. R. Paul, "Literal solutions for time-domain crosstalk on lossless transmission lines," *IEEE Trans. Electromagn. Compat.*, vol. 34, no. 4, pp. 433–444, Nov. 1992.

[7] Y.-Z. Xie, J. Guo, and F. Canavero, "Analytic iterative solution of electromagnetic pulse coupling to multiconductor transmission lines," *IEEE Trans. Electromagn. Compat.*, vol. 55, no. 3, pp. 451–466, Jun. 2013.

[8] R. Achar, M. Nakhla, A. Sridhar, H. Dhindsa, and D. Paul, "Fast analysis of power distribution networks using waveform relaxation," in *IEEE Workshop Signal Propag. Interconnects*, May 2009, pp. 1–4.

[9] N. Nakhla, A. E. Ruehli, M. S. Nakhla, R. Achar, and C.-Z. Chen, "Waveform relaxation techniques for simulation of coupled interconnects with frequency-dependent parameters," *IEEE Trans. Adv. Packag.*, vol. 30, no. 2, pp. 257–269, Feb. 2007.

[10] M. A. Farhan, N. M. Nakhla, M. S. Nakhla, R. Achar, and A. E. Ruehli, "Overlapping partitioning techniques for simulation of strongly coupled distributed interconnects," *IEEE Trans. Compon. Packag. Manuf. Technol.*, vol. 2, no. 7, pp. 1193–1201, Jul. 2012.

[11] V. Loggia, S. G. Talocia, and H. S. Hu, "Transient simulation of complex high-speed channels via waveform relaxation," *IEEE Trans. Compon. Packag. Manuf. Technol.*, vol. 1, no. 11, pp. 1823–1838, Nov. 2011.

[12] R. Achar, M. S. Nakhla, H. S. Dhindsa, A. R. Sridhar, D. Paul, and N. M. Nakhla, "Parallel and scalable transient simulator for power grids via waveform relaxation (PTS-PWR)," *IEEE Trans. Very Large Scale Integr. Syst.*, vol. 19, no. 2, pp. 319–332, Feb. 2011.

[13] N. Nakhla, A. Ruehli, M. S. Nakhla, and R. Achar, "Simulation of coupled interconnects using waveform relaxation and transverse partitioning," *IEEE Trans. Adv. Packag.*, vol. 29, no. 1, pp. 78–87, Feb. 2006.

[14] A. R. Sridhar, N. M. Nakhla, R. Achar, M. S. Nakhla, and A. E. Ruehli, "Fast EMI analysis via transverse partitioning and waveform relaxation," *IEEE Trans. Electromagn. Compat.*, vol. 51, no. 2, pp. 358–371, May 2009.

[15] I. M. Elfadel, "Convergence of transverse waveform relaxation for the electrical analysis of very wide transmission line buses," *IEEE Trans. Comput.-Aided Design Integr. Circuits Syst.*, vol. 28, no. 8, pp. 1150–1161, Aug. 2009.

[16] H. Dhindsa, A. Sridhar, R. Achar, M. Nakhla, and D. Paul, "Transient analysis of power grid networks via waveform relaxation techniques," in *Proc. Int. Microw. Workshop Ser. Signal Integrity High-Speed Interconnects*, Feb. 2009, pp. 91–94.

[17] S. Roy and A. Dounavis, "Delay-extraction-based waveform relaxation algorithm for fast transient analysis of power distribution networks," *IEEE Trans. Compon. Packag. Manuf. Technol.*, vol. 2, no. 12, pp. 2044–2056, Dec. 2012.

[18] S. Roy and S. A. Dounavis, "Parallel transient simulation of package/board power distribution networks based on a 2-D overlapping partitioning methodology," *IEEE Trans. Compon. Packag. Manuf. Technol.*, vol. 3, no. 12, pp. 2101–2112, Dec. 2013.

[19] S. Roy, A. Beygi, and A. Dounavis, "Electromagnetic interference analysis of multiconductor transmission line networks using longitudinal partitioning-based waveform relaxation algorithm," *IEEE Trans. Electromag. Compat.*, vol. 55, no. 2, pp. 395–406, Apr. 2013.

[20] S. Roy and A. Dounavis, "Waveform relaxation based analysis of noise propagation in power distribution networks propagation in power distribution networks," in *Proc. IEEE 20th Conf. Electr. Perform. Electron. Packag. Syst.*, 2011, pp. 255–258.

[21] M. A. Khaleel, A. E. Ruchli, and M. J. Gander, "Optimized waveform relaxation methods for longitudinal partitioning of transmission lines," *IEEE Trans. Circuits Syst. I, Reg. Papers*, vol. 56, no. 8, pp. 1732–1743, Aug. 2009.

[22] R. Achar and M. S. Nakhla, "Simulation of high-speed interconnects," *Proc. IEEE*, vol. 89, no. 5, pp. 693–728, May 2001.

[23] Y.-Z. Xie, F. Canavero, T. Maextri, and Z.-J. Wang, "Crosstalk analysis of multiconductor transmission lines based on distributed analytical representation and iterative technique," *IEEE Trans. Electromagn. Compat.*, vol. 52, no. 3, pp. 712–727, Aug. 2010

[24] Y.-Z. Xie, F. G. Canavero, T. Maestri, and Z.-j. Wang, "Analytic iterative approach to crosstalk analysis of multiconductor transmission lines," in *Proc. Eur. Symp. Electromagn. Compat.*, 2010, pp. 775–780.

[25] C. E. Baum, T. K. Liu, and F. M. Tesche, "On the analysis of general multiconductor transmission line networks," Interaction Note 350, 1978.

[26] J. Guo, Y.-Z. Xie, K.-J. Li, and F. Canavero, "Convergence analysis of the distributed analytical representation and iterative technique (DARIT-field) for the field coupling to multiconductor transmission lines," *IEEE Trans. Electromagn. Compat.*, vol. 5, no. 6, Dec. 2014.